Aerodynamic benefits of drafting in speed skating

Estimates from in-field skater's wakes and wind tunnel measurements

Terra, Wouter; Spoelstra, Alexander; Sciacchitano, Andrea

DOI
10.1016/j.jweia.2023.105329

Publication date
2023

Document Version
Final published version

Published in
Journal of Wind Engineering and Industrial Aerodynamics

Citation (APA)
Terra, W., Spoelstra, A., & Sciacchitano, A. (2023). Aerodynamic benefits of drafting in speed skating: Estimates from in-field skater's wakes and wind tunnel measurements. *Journal of Wind Engineering and Industrial Aerodynamics*, *233*, Article 105329. https://doi.org/10.1016/j.jweia.2023.105329

Journal of Wind Engineering & Industrial Aerodynamics 233 (2023) 105329

Contents lists available at ScienceDirect

Journal of Wind Engineering & Industrial Aerodynamics

journal homepage: www.elsevier.com/locate/jweia

Aerodynamic benefits of drafting in speed skating: Estimates from in-field skater's wakes and wind tunnel measurements

Wouter Terra [a,*], Alexander Spoelstra [b], Andrea Sciacchitano [b]

[a] TeamNL Experts, NOC*NSF, the Netherlands
[b] Aerospace Engineering Department, Delft University of Technology, the Netherlands

A B S T R A C T

The effect of drafting on the aerodynamic drag of a long-track speed skater is investigated in-field, at the 400m ice-rink of Thialf, Heerenveen. The Ring of Fire system is used to measure the flow downstream of an elite, isolated skater at approximately 11 m/s, transiting repeatedly through a tunnel filled with Helium-filled soap bubble flow tracers. Large-scale stereoscopic particle image velocimetry is used at an acquisition frequency of 500 Hz to obtain the near to far wake up to 11 m distance behind the skater. Over these 11 m, the center of gravity of the wake can shift up to 10 cm laterally, depending on the phase of the skating motion, and it moves about 15 cm to the floor. The former suggests that a trailing skater should slightly adapt its trajectory to achieve the lowest aerodynamic drag by drafting. The drag reduction of a trailing skater is estimated from the measurements on the isolated rider, assuming that the trailing rider's drag reduction only stems from the loss in total pressure in the wake of the first rider. The drag reduction is obtained with varying lateral and longitudinal distance between the leading and hypothetical trailing rider. It is observed that the peak reduction (~40%) steeply decays with increasing lateral offset: at an offset of 50 cm the reduction is negligible. Instead, with increasing longitudinal offset, the decay is more gradual: at a distance of 11 m the reduction of 17% remains significant. The in-field estimations of the drag reduction are supported by wind tunnel measurements conducted on scaled skater models. Finally, the results obtained on the ice-rink indicate that a trailing skater should follow a slightly wider trajectory of about 20 cm, in comparison to the leading skater, to achieve the peak drag reduction during the entire skating stroke.

1. Introduction

In long-track speed skating, the aerodynamic drag may contribute to 90% of the overall resistance the athlete has to overcome (Oggiano and Sætran, 2010). Hence, reduction of the aerodynamic drag can be an efficient way to enhance athlete performance. For a skater, drafting is arguably the most efficient way to reduce his or her aerodynamic drag: It can lead to reductions of the aerodynamic drag of over 20% (Van Ingen Schenau, 1982). Although drafting in long-track speed skating may not be as common as it is in cycling, it is relevant in several disciplines, such as the team pursuit, the team sprint and the mass-start and in individual races as well, when two riders are crossing lanes. Nevertheless, little is known about the effects of drafting in speed skating. Van Ingen Schenau (1982) reported a drag reduction of a trailing skater, compared to an isolated skater, of 23% and 16% at 1 and 2 m, respectively, behind a leading skater. Other studies report, among others, reduced heart rate when skating behind a leading skater in long track (van der Brandt et al., 2021) as well as short-track skating (Rundell, 1996). The number of works on the effect of drafting in speed skating is certainly small compared to that available in the cycling literature. Drafting effects on cycling aerodynamic drag have been reported, among others, for group sizes of two (Blocken et al., 2013), four (Broker et al., 1999) and more riders (Blocken et al., 2018), for varying order of riders of different composition (Barry et al., 2015), for different longitudinal and lateral distances between riders (Barry et al., 2014; Spoelstra et al., 2021) and in the presence of cross wind (Belloli et al., 2016). Also the interaction of two riders from the perspective of the fluid is reported (Barry et al., 2016) as well as the reduction of the dynamic pressure downstream of a single cyclist (e.g. Crouch et al., 2014; Brown et al., 2020), being the main source of drag reduction of a trailing cyclist. This illustrates that much is yet unknown about drafting in speed skating and this work aims to provide further insight into this.

A particular difference between cycling and skating, is that during the former the rider generally travels along a straight trajectory, while in the latter case the body of the athlete follows a harmonic trajectory, continuously moving forward in addition to a sideways motion alternatingly to the left and to the right (van der Kruk, 2018). The skater's body posture varies continuously during this repetitive motion of skating strokes affecting the flow around the athlete and, therefore, the aerodynamic drag reduction by drafting of a possible trailing skater. Hence, this work aims to investigate the effect of drafting in speed skating by measurements on an actual skating athlete on the ice. To do so, first the wake of a skater in isolation is characterized using the Ring of Fire system. This in-field measurement system adopts large-scale

* Corresponding author.
E-mail address: w.terra@tudelft.nl (W. Terra).

https://doi.org/10.1016/j.jweia.2023.105329
Received 14 September 2022; Received in revised form 11 January 2023; Accepted 22 January 2023
Available online 31 January 2023

particle image velocimetry (PIV) to measure the flow past transiting objects and has been used previously in cycling (Spoelstra et al., 2019, 2021) as well as in speed skating (Spoelstra et al., 2022). Secondly, this wake information is used to estimate the drag reduction of a potential trailing skater similar to Brown et al. (2020) and Spoelstra et al. (2021). The presented drag reduction estimates, obtained from the wake of a skater in isolation, are finally compared to wind tunnel balance measurements on a tandem of skater mannequins at scale 1:5.

2. Methodology

The aerodynamic drag, D acting on an object immersed in a fluid results from the relative velocity between the two and is defined as:

$$D = 1/2\rho U_\infty^2 C_D A \tag{1}$$

with ρ being the air density of the fluid, U_∞ the freestream velocity (relative speed between object and fluid) and C_D and A the object's drag coefficient and projected frontal area. The aerodynamic drag acting on a model can be reduced by placing another model upstream of it, which is generally referred to as drafting. The resulting drag reduction, DR can be expressed as the relative difference between the aerodynamic drag of the model in isolation, D_{single} and that when drafting, D_{draft}:

$$DR\ [\%] = 100 \bullet \frac{D_{single} - D_{draft}}{D_{single}} \tag{2}$$

where the aerodynamic drag of the model in isolation is obtained from Equation (1) with $C_D = C_{D,single}$. For the aerodynamic drag of the trailing model, a similar expression can be used:

$$D_{draft} = 1/2\rho U_\infty^2 C_{D,draft} A \tag{3}$$

This expression suggests that the drag reduction of the trailing model results solely from a reduction in drag coefficient of the latter, $C_{D,draft}$. In practise, however, the flow approaching the trailing model is generally non-uniform and the streamwise velocity is smaller than that in the freestream $U_{draft}\ (y,z) \leq U_\infty$. As a result, the total pressure upstream of the trailing model and its aerodynamic drag is reduced.

In cycling, the flow topology around an isolated rider is similar to that around the trailing rider in tandem configuration (Barry et al., 2016). Hence, it is assumed that $C_{D,draft} \sim C_{D,single}$ and that the aerodynamic drag reduction by drafting is dominated by the modified total pressure in between the two models. When assuming that the flow in between two riders in tandem configuration is the same as the flow downstream of a single one, the drag reduction by drafting can be estimated from the wake information of the leading cyclist, riding in isolation, and the projected frontal area of the trailing rider. Brown et al. (2020) use the relative difference between the freestream dynamic pressure, Q_∞ and the time-average dynamic pressure in the wake of the single, leading rider $\overline{Q}_{wake}$ to define the drag reduction:

$$DR\ [\%] = 100 \bullet \iint \frac{Q_\infty - \overline{Q}_{wake}}{Q_\infty} dA \tag{4}$$

Instead, in this work the relative difference in total pressure is used, similar to Spoelstra et al. (2021), which also accounts for a reduction of the aerodynamic drag of the trailing athlete as a consequence of the low pressure region in the wake of the leading one, in addition to that of the change of the dynamic pressure. Furthermore, the drag reduction by drafting is estimated from instantaneous wake information, instead of time-averaged. Hence, the expression for the drag reduction becomes:

$$DR\ [\%] = \iint \frac{P_{tot,\infty} - P_{tot,wake}}{P_{tot,\infty}} dA \tag{5}$$

where $P_{tot,\infty}$ equals the total pressure in the freestream and $P_{tot,\ wake}$ the instantaneous total pressure in the wake of the single, leading skater. Because the present methodology does not include interaction effects in the flow between two skaters, the drag reduction is underestimated by about 10% (Spoelstra et al., 2021). In addition to the error stemming from the present method, the error that is introduced in the computation of the aerodynamic drag with the Ring of Fire is approximately 5% (Spoelstra et al., 2020). Through linear error propagation of these two sources of error, the upper and lower bound of the uncertainty of the estimated drag reduction become 5% and 11%, respectively.

3. Experimental apparatus and procedures

The data that was acquired in February 2021 at the Thialf ice arena in Heerenveen in the Netherlands, described by Spoelstra et al. (2022), also forms the basis for the present work. Hence, the test facilities, participants and experimental apparatus are the same as those described in the work of Spoelstra et al. and, therefore, are not described here in detail. Only the most relevant parts are listed and the reader is referred to the latter work for more details. In addition to the Ring of Fire experiments, wind tunnel measurements are conducted on scaled skater models to compare the estimated drag reduction from the first to the latter. These wind tunnel tests are described in the end of this section.

3.1. Ring of Fire: Test facility and subjects

For the present work, a single male professional skater participated in the experiment at the 400-m ice rink of Thialf. His body mass and height were in the range of 75–80 kg and 175–180 cm (exact number are

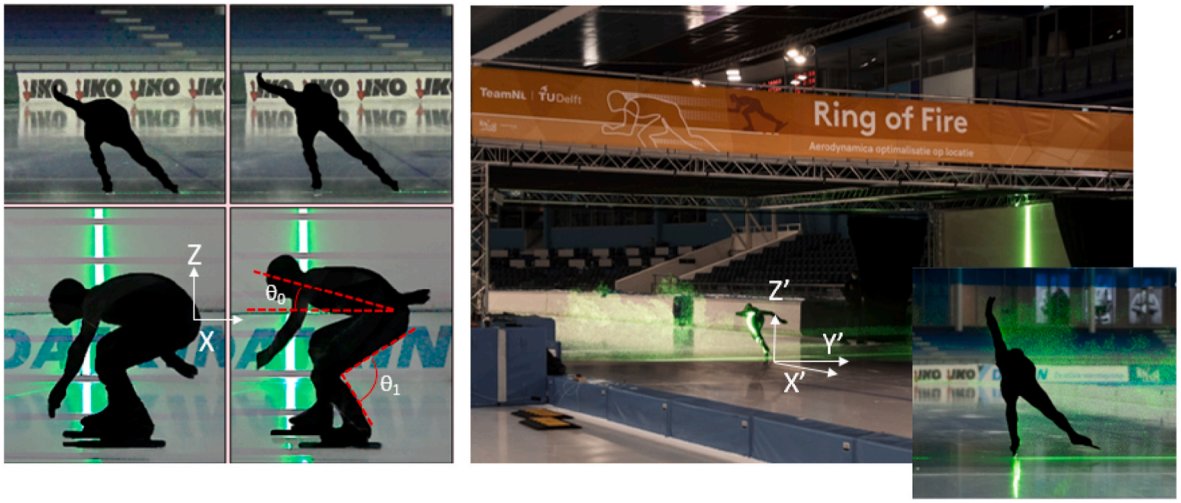

Fig. 1. The two skating postures (left) and the athlete transiting through the Ring of Fire (right).

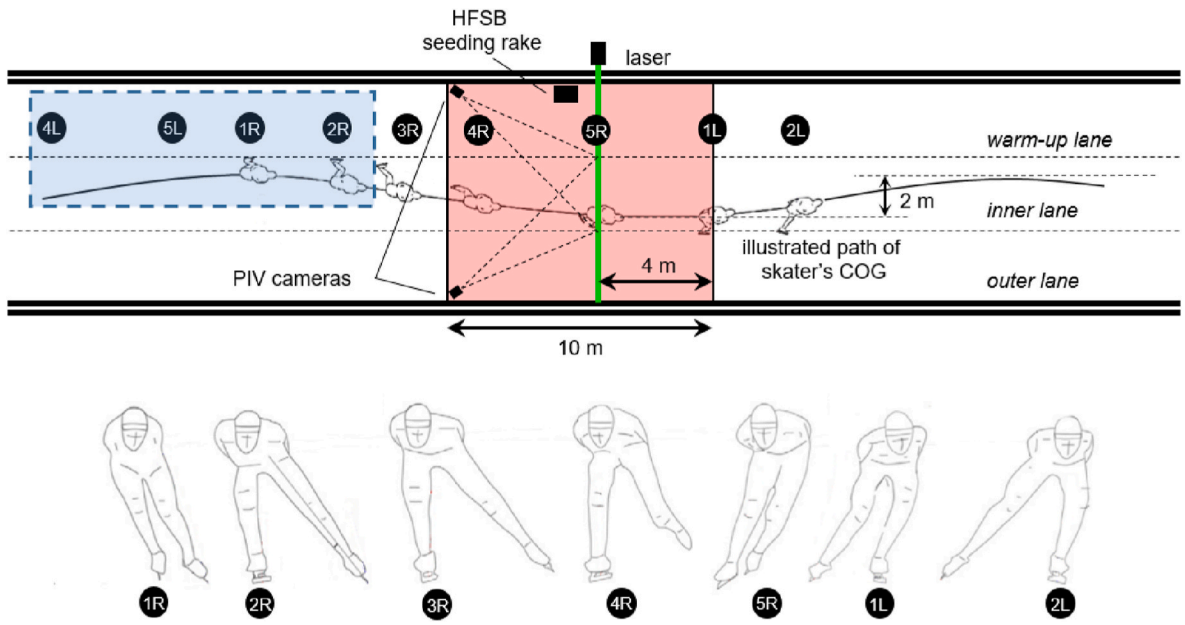

Fig. 2. A schematic of the Ring of Fire system including an illustration of a skater's trajectory and of the skater's posture along that path (top) and frontal views, marked 1 to 5 and moving left (L) or right (R), views of the postures (bottom). The illustration of the skating postures are adapted from Van der Kruk (2018). The dashed blue box marks the postures in which the skater actually passed through the measurement region.

not reported for confidentiality reasons); during all tests he wore a typical speed skating skinsuit and laser safety goggles for protection against the PIV laser light. Two different skating configurations are considered in this work: a high trunk and a low trunk posture. The trunk angle, θ_0, knee angle, θ_1 and frontal area, A of the skater (Fig. 1-right) in the high trunk and low trunk posture were approximately [$\theta_0 = 16°$; $\theta_1 = 92°$; A = 0.31 m^2] and [$\theta_0 = 0°$; $\theta_1 = 84°$; A = 0.28 m^2]. The knee angle is measured on the standing leg in the push-off phase of the skating stroke (phase 2 in Fig. 2).

3.2. The Ring of Fire: System apparatus

The Ring of Fire system is used to measure the air velocity prior to and after the transit of the skater. Large-scale stereoscopic PIV is adopted to measure the flow in a plane, orthogonal to the direction of the skating lanes, of approximately 7 m^2. A tunnel of 10 × 13 × 3 m^3 in X', Y', and Z' direction (see Fig. 1-right) was used to confine the neutrally buoyant helium-filled soap bubbles (HFSB) within the measurement area. Before the transit of the skater, tracer particles were accumulated for about 2 min by closing the entrance and exit gates of the tunnel. The HFSB were introduced into the tunnel by a rake with 200 nozzles and the tracers were imaged (two Photron Fast CAM SA1 cameras) and illuminated (Quantronix Darwin Duo Nd:YAG laser) at a frequency of 0.5 kHz. The reference system ($X'Y'Z'$) is defined relative to the Ring of Fire system (Fig. 1-right), with X′$_0$, Y′$_0$ and Z′$_0$ coinciding with the location of the measurement plane, the middle of the inner lane and the ice-floor, respectively. A second reference system, (XYZ) is introduced moving with the skater with its origin located at its lower back (see Fig. 1-left). Table 1 summarizes the PIV experimental apparatus including imaging and acquisition parameters.

Table 1
Experimental equipment, imaging and acquisition parameters.

Equipment		
Purpose	Instrument	
Imaging	Cameras	2 × Photron Fast CAM SA1 cameras (CMOS, 1024 × 1024 pixels, pixel pitch 20 μm, 12 bits)
	Objectives	2 × Nikon $f = 50$ mm
	Other	Bandpass filter (532 nm)
Illumination	Laser	Quantronix Darwin Duo Nd:YAG laser (2 × 25 mJ at 1 kHz)
Seeding	Seeding particles	Neutrally buoyant Helium-filled soap bubbles
	Seeding system	200 nozzles

Imaging and acquisition parameters		
Purpose	Parameter	
Field of view	X (thickness) [m]	0.05
	Y (width) [m]	4
	Z (height) [m]	2.9
Imaging	$f_\#$	5.6
	Sensor cropped to	1024 × 752 pixels
	Magnification	0.005
	Digital image resolution [mm/px]	3.8
Measurement rate	f_{acq} [Hz]	500
Seeding concentration	Particle imaging density [ppp]	0.1

3.3. Ring of Fire: Experimental procedures

The athlete passed 19 times through the Ring of Fire, 10 times in the low trunk and 9 times in the high trunk configuration. The ability of the skater to reproduce these configurations, passage after passage, is evaluated based on the position of the lower back and that of the head. The vertical location above the ice (Z′) and the lateral position with respect to the centre of the inner lane (Y′) are measured using the raw images acquired by the PIV cameras (Fig. 3). These coordinates are all listed in the appendix. The lateral location of the goggles is measured from the frame when the head is just entering the measurement plane (left figure). This frame is recognized by the first appearance of the shadows of the head, which is marked in the figure. The frame that marks the moment when the buttocks are just about to leave the measurement plane is indicated in the right figure (in the frame after no reflection on the buttocks is observed). In these raw images, the illuminated HFSB can also be observed as the bright spots. The very bright line on the lower part of the images is a consequence of the laser light illuminating the ice.

The skater was well able to reproduce the low and high trunk configuration and the configurations are significantly different in the position of the lower back and head. Among the low trunk passages, the

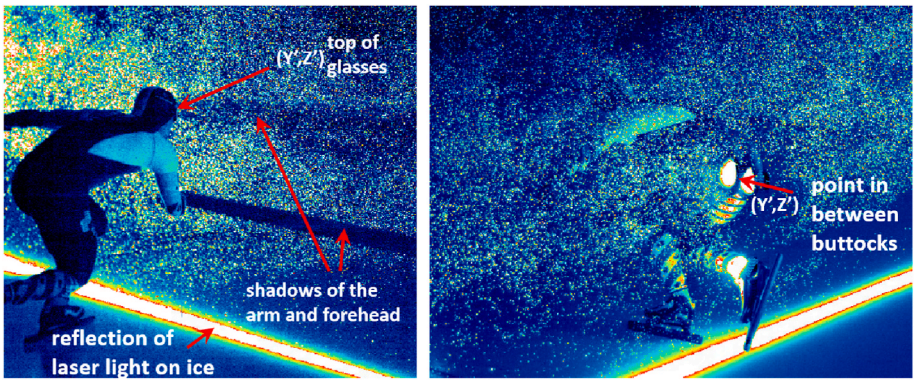

Fig. 3. Raw images of the PIV cameras of the skater's head entering the measurement plane (left) and the buttocks leaving it (right).

average vertical distance of the lower back to the ice was $Z' = 72$ cm with a standard deviation of 1.2 cm. In the high trunk configuration this was $Z' = 77$ cm with a standard deviation of 1.6 cm. The position of the head in the low and high trunk configurations was $Z' = 84$ cm and $Z' = 101$ cm with standard deviations of 1.5 and 2.9 cm, respectively. For all trials, the athlete started on the opposite straight part of the track, accelerated to the prescribed velocity of 11 m/s and maintained such velocity in the corner and along the second straight part of the track; he changed his posture and speed only at the beginning of the second corner, after having passed the measurement domain. Based on the skater's speed and shoulder width SW = 0.5 m, the resulting Reynolds number was about $Re = 3.5 \times 10^5$. The skater's speed, u_A was measured with the ProChip Timing System by MYLAPS Sports Timing installed in Thialf and its posture was monitored by two cameras (additional to those of the PIV system): one providing a side view (Fig. 1 bottom-left) and the other a frontal view of the athlete (Fig. 1 top-left).

3.4. Ring of Fire: Data reduction

Based on the skating phase in which the rider passed through the measurement plane, each passage of the rider is categorized. Following Spoelstra et al. (2022), five different skating phases are considered. In addition, each phase can be within a left or a right stroke and, so, we end up with 10 different categories (phase 1L–5L and 1R–5R; see Fig. 2). In the present experiments, the rider passed through the measurement plane in phases [4L 5L 1R 2R] only, which have been marked blue in Fig. 2 top.

Furthermore, 20 consecutive image pairs, acquired about 0.4 s prior to each passage of the skater, are processed to obtain the velocity distribution of the undisturbed air. First background reflections and noise are reduced via a temporal filter, before a time-resolved stereo-PIV cross-correlation algorithm is applied with a final interrogation window size of 32 × 32 pixels (100 × 100 mm^2) and an overlap of 75%. The obtained velocity fields are averaged to obtain a robust estimate of the undisturbed conditions. So far, the experimental facility, equipment and procedures were the same as that of Spoelstra et al. (2022). The processing of the acquired PIV data after passage of the skater, instead, is different from that work. To avoid spurious vectors that would otherwise result from occasional lack of seeding in small regions in the measurement plane, the 500 consecutive image pairs acquired after the passage of the rider are processed using a stereo-PIV sliding sum-of-correlation algorithm (Sciacchitano et al., 2012; kernel of 7) after a background subtraction processing step. Another advantage of using the sliding sum-of-correlation algorithm is the reduction of PIV error by a factor 3 though in increase in the correlation signal strength and attenuation of the amplitude of noisy velocity fluctuations. The size of the interrogation window and the overlap factor are the same as those used to process the images before the skater's passage. The first of this set of images is marked by the moment the lower back of the skater exits the laser sheet. At this time, $t = 0$ the streamwise coordinates of the two coordinate systems overlap: $X = X' = 0$. An error of about 2 μs is introduced by this selection procedure (governed by the acquisition frequency). This error propagates into the phase-average velocity fields: with $u_A = 11$ m/s, the error in the streamwise coordinate X is about 2 cm. The measurement area, containing sufficient seeding for the PIV analysis, is [−1 to 3] m and [0 to 1.6] m along Y′ and Z′, respectively.

Finally, in the present work the velocity downstream of a skater is measured in a frame of reference fixed to the ice rink ($X'Y'Z'$). Instead, the drag reduction is calculated using Equation (5), which is expressed in the frame of reference moving with the skater (XYZ). Hence, to interchange time and distance between these two reference frames, we make the assumption of a quasi-steady wake, while in reality it is continuously transient. The same assumption is made when presenting the measured velocity in the reference frame (XYZ).

3.5. Force balance measurements on a scaled model

To complement the on-site measurements on real athletes, experiments on scale models are conducted in the W-tunnel of the Aerodynamics Laboratories of TU Delft. This low-speed, open-jet wind tunnel has an exit cross-section of 0.6 × 0.6 m^2 and turbulence intensity level below 1%. The skater model has been created in MakeHuman and, afterwards, articulated into a position that resembles phase 2R (two arms loose) of the skating motion (Fig. 4-top-left) using Blender. The trunk and knee angles are approximately $\theta_0 = 11°$; $\theta_1 = 83°$, respectively. The model geometry is freely available at the 4TU data repository (Terra et al., 2022). A physical mannequin (approximately scale 1:5) that is 30 cm wide and 20 cm high along [Y,Z] is created using additive manufacturing; no garment is applied to the mannequin during the tests.

Measurements are conducted on a skater in isolation and with two skaters: one skater drafting behind a leading one. In the latter case, the lateral and longitudinal offset between the models is varied in a range of -10 cm $< \Delta Y <$ 10 cm and $0 < \Delta X <$ 70 cm, respectively, with $\Delta Y = 0$ being the situations with the two models aligned along the Y-axis and $\Delta X = 0$ is the situation where the distance between the lower back of the leading skater and the hand of the second skater is just not touching (about 2 mm). These offsets are changed by moving the leading model only throughout the closed-section wind tunnel area, while the second skater remains in a fixed position attached to a ground plate (marked red in Fig. 4). To do so, the leading model is installed on a 2 mm thick steel plate (marked blue in Fig. 4-left), which is fixed to the wind tunnel floor using tape. To compare the results from the wind tunnel to those from the ice-rink, the dimensions of ΔX and ΔY of the former are rescaled to match those of the latter. All measurements are conducted at a free-stream velocity of 17 m/s. The corresponding Reynolds number, $Re = 9 \times 10^4$ based on the shoulder width (SW = 8 cm), is about a factor four below that of the Ring of fire experiments. Furthermore, the wind tunnel solid blockage ratio is between 4% (single model) and 7% (two models)

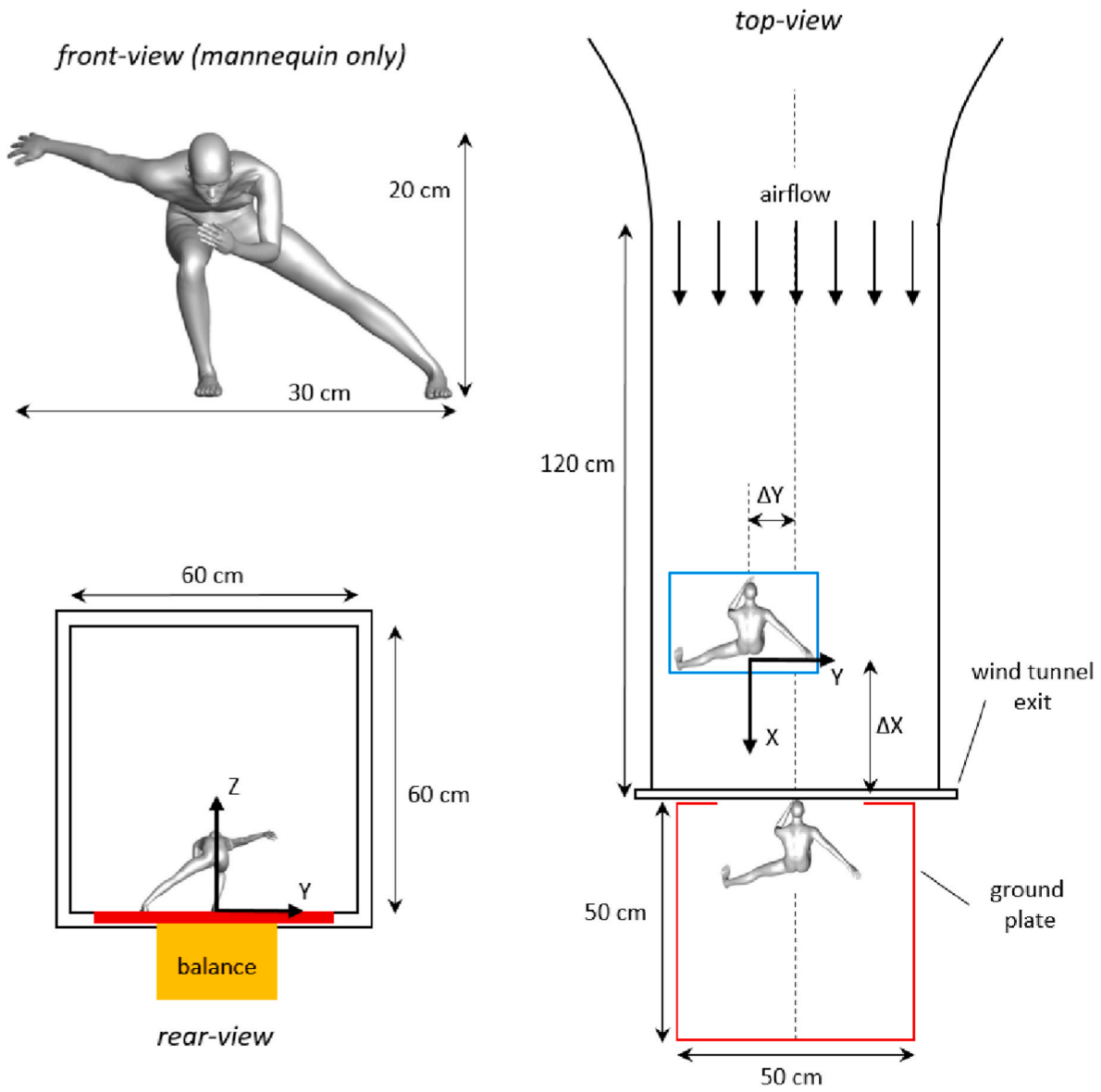

Fig. 4. Layout of experiments: The skater model (top-left); illustration of a single skater (bottom-left) and a two-skater setup (right).

and that of the in-field tests is about 1%. Blockage corrections have not been applied, as the uncertainty resulting from such corrections is of the same order of magnitude as the blockage effect itself.

A home-made two-component balance (Huang et al., 2022), which is marked orange in Fig. 4, consists of three load cells of type: KD40s (max range ±50N, max error: ≤0:1%). Two of the load cells measure the streamwise force while the other one measures the lateral force. On top of the balance, a ground plate is mounted flush with the wind tunnel test section floor (marked red). A small gap of about 3 mm was present between the wind tunnel exit and the plate. All balance measurements are conducted at 2 kHz for an observation time of 30 s, leading to 60,000 samples per run. Finally, a wind tunnel repetition test was conducted, during which the leading skater model was removed and reinstalled three times in the test section and the wind tunnel was stopped and started in between. The resulting values of the drag coefficient of the trailing model were in a range of 0.25% of each other.

4. Results

Following the work of Spoelstra et al. (2022) for cycling, we assume that the drag reduction experienced by a drafting skater is dominated by the change in the total pressure downstream of the leading skater and, so, that this drag reduction can be estimated from the wake information measured on a single skater (e.g. Equation (5)). In this section, the near-to far-wake of such a single skater is described to understand how the drag reduction of a hypothetical trailing skater may be affected, among others, by the longitudinal and lateral offset to the leading skater. After that, the actual drag reduction estimates are presented and compared to force balance measurements on scaled models in the wind tunnel. The data underlying the results presented in this work is freely available at the 4TU repository (Terra et al., 2022).

4.1. Qualitative description of the wake of the single skater

During the present experiments, the air in the measurement domain prior to the passage of the skater was not fully stagnant. The actual flow velocities experienced by the rider are described by Spoelstra et al. (2022). They report significant out-of-plane and in-plane velocities (up to 20 cm/s) in the area $Y' < 1$ m and $Z' > 1$ m as a consequence of the HFSB injection; conversely, in the remaining area, the out-of-plane velocities are within ±2.5 cm/s and the in-plane velocities are close to zero. Although the largest part of the wake of the skater is in the latter

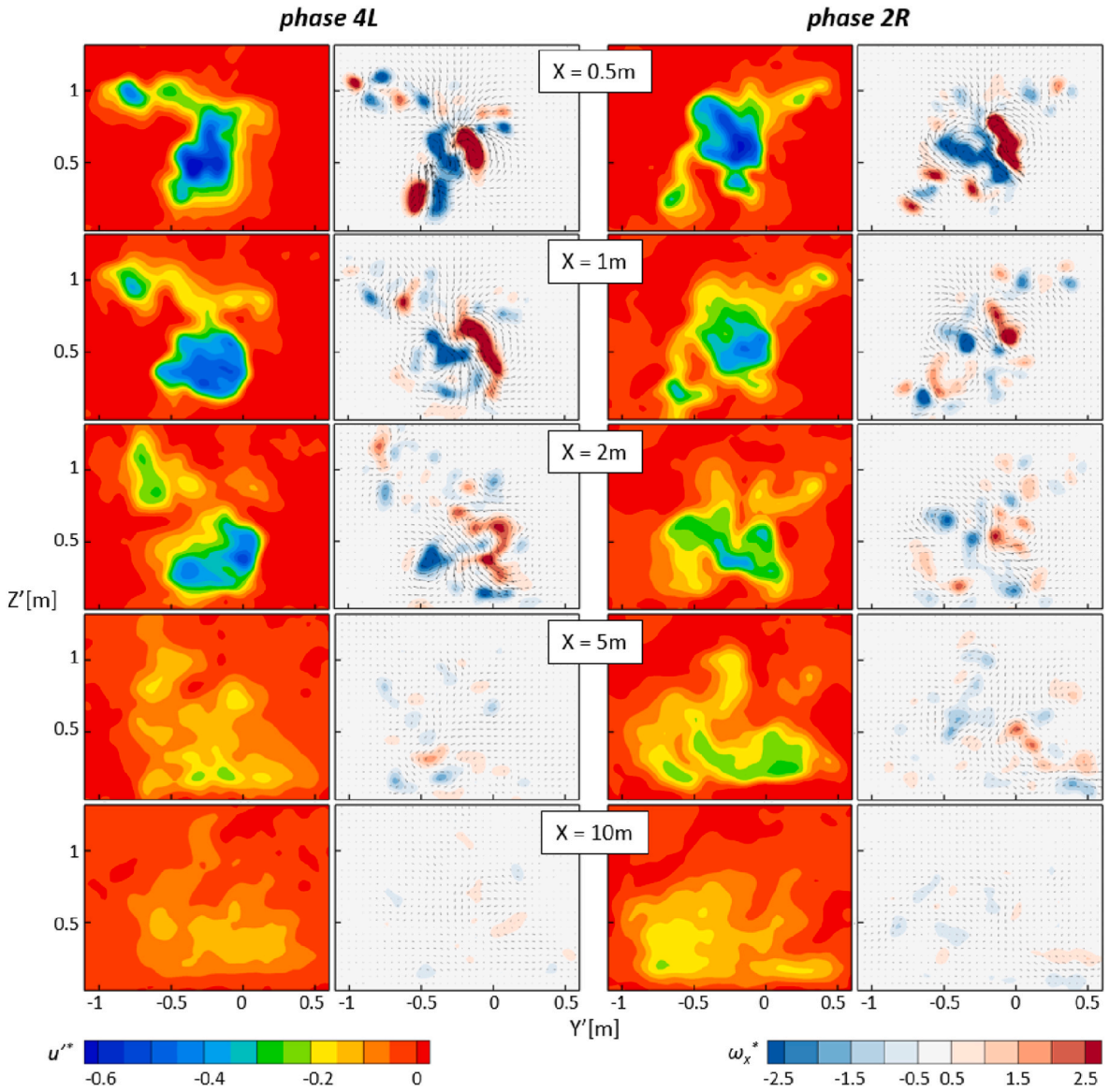

Fig. 5. Distribution of non-dimensional streamwise velocity (1st and 3rd column) and vorticity (2nd and 4th column) downstream of the skater.

region, and so the freestream velocity can be considered uniform, it should be reminded that the flow tracer injection might have a small effect on the skater's wake distributions presented in Fig. 5. This figure presents the non-dimensional streamwise velocity, $u'^{*} = \frac{u'}{|u_A|}$ and non-dimensional vorticity distribution, $\omega_x^* = \frac{\omega_x c}{|u_A|}$ in the laboratory frame of reference, with c being a characteristics length chosen equal to the shoulder width of the skater (SW = 0.5 m). The time instants of the snapshots that are depicted are in the frame of reference moving with the skater ($X = u_A \bullet t$), which implies the assumption of a quasi-steady wake. For reasons of conciseness, we do not present the wake evolution of all four phases. Instead, two individual passages of the skater in the low-trunk configuration are depicted, one in phase 4L and one in phase 2R, which are about half a stroke length apart (see Fig. 2). For the sake of readability, these images have been cropped to an area of [−1.6 to 0.1] m and [0 to 1.4] m along Y′ and Z′, respectively.

It is observed that towards the boundaries of the depicted area the streamwise velocity is close to zero (red area in first and third column), indicating undisturbed flow. In the center of the skater's wake, instead, peaks of streamwise velocity are observed of $u'^{*} = -0.6$ at X = 0.5m (indicated in dark-blue), which decays to about $u'^{*} = -0.15$ at X = 10m. In Fig. 5 top-left, a region of high velocity deficit is observed in phase 4L downstream of the left arm swinging to the left, while in phase 2R, such an area is located behind the right arm swinging to the right. In the latter case, the wakes of the two individual legs are clearly visible, while in the former, the wakes of the legs have somehow merged. In other words, the posture of the skater can be recognized well from the velocity distribution in its near-wake. Because of turbulent dissipation, this is not the case anymore in the far-wake. Hence, in agreement to Spoelstra et al. (2022), the velocity distribution, measured shortly downstream to the rider, is strongly dependent on the corresponding skating phase. It is also observed that the vertical position of the overall velocity distribution moves towards the ice floor when moving further away from the skater. Instead, the lateral position seems relatively unaltered. This evolution of the wake center of gravity is quantified later in this section (Fig. 7).

The distribution of the streamwise vorticity behaves somehow similarly to that of the velocity: The peak in vorticity decays with increasing X and the posture of the skater can be observed in its distribution at X = 0.5. Furthermore, for both skating phases, one counter-rotating vortex pair, seemingly originating from the hips or lower back, dominates the near-wake topology, while small vortex pairs emanate from the arms and legs. All these vortex structures, however,

dissipate and merge rather quickly and, after X = 5 m, it is not evident anymore how to relate the vorticity distribution to that in the near-wake. Finally, it should be noted, that the velocity distributions measured at X > 2m ($t > 0.2$s) are not governed anymore by the posture of the skater when passing through the measurement plane, but instead by postures earlier in the skating stroke.

4.2. Statistical evaluation of the skater's wake

In order to obtain an understanding of the downstream evolution of the skater's wake, two different passages in different skating phases through the present measurement system have been considered. As a consequence of the relatively small ensemble of passages per skating phase, it is not possible to present a statistically converged wake topology. In order to investigate the similarities and the differences among all 19 passages, some general wake statistics are presented so to obtain a better understanding of how a hypothetical trailing skater can best 'harvest' the momentum in the wake of a leading skater. Fig. 6 depicts the maximum and average non-dimensional streamwise velocity, u'^*_{max} and u'^*_{mean} respectively, against increasing time (top horizontal axis) and increasing distance to the skater (bottom horizontal axis). These velocities are computed within the wake area, being the region containing air that is disturbed by the passage of the skater and, so, being bounded by undisturbed air. The contouring method of Spoelstra et al. (2020) is adopted to define this wake area. The value of u'^*_{max} (Fig. 6-left) is around 60% immediately downstream of the skater and decays quickly afterwards to 20% at a distance of 11 m. The relatively small standard deviation, depicted by the error bars, demonstrates that the decay of u'^*_{max} among the different passages follows the same trend and, hence, is not much affected by the skating phase or the skating configuration (high or low trunk). The decay of the mean streamwise velocity is less steep, from about 10% to 5% over 11 m (Figure-6 right). Among the passages, also the decay of the mean wake streamwise velocity is within a relatively small error band, although it is higher than that of the maximum velocity. Partly, this is a consequence of the wake contouring method that determines the wake area, which introduces an additional variable among all the passages. Nevertheless, it can be concluded that the evolution of both wake parameters seems relatively independent of the skating phase. Therefore, based on these statistics, it can be expected that the drag reduction of a hypothetical skater that is immersed in the wake of a leading one is quite similar among the skating phases.

Apart from the maximum and mean streamwise velocity, also the lateral and vertical locations of the center of the wake are evaluated to find the best position for a trailing skater to reduce its aerodynamic drag. It was already observed that the wake of a skater remains in a relatively fixed lateral position (considered in the laboratory frame of references; Fig. 5) and, instead, moved closer to the ice-floor further downstream of the athlete. To quantify the wake displacement, the center of mass or center of gravity of the wake is calculated. This method is also commonly adopted in the analysis of wind turbines (e.g. Howland et al., 2016) and it defines the lateral, $Y'_{CG,wake}$ and vertical position of the wake center of gravity, $Y'_{CG,wake}$ as:

$$Y'_{CG,wake} = \frac{\iint u(Y',Z')Y'\,dS_{wake}}{\iint u(Y',Z')dS_{wake}};\qquad Z'_{CG,wake} = \frac{\iint u(Y',Z')Z'\,dS_{wake}}{\iint u(Y',Z')dS_{wake}} \tag{6}$$

The displacement of the wake center of gravity in lateral, $\Delta Z_{CG,wake}$ (Fig. 7-left) and in vertical direction, $\Delta Y_{CG,wake}$ (Fig. 7-right) are presented relative to the location of the lower back of the skater when passing through the measurement plane. The method to determine the location of the lower back is described in Section 3 and illustrated in Fig. 3. The absolute location of the wake at X = 0 of all individual passages are listed in the appendix. Instead of presenting the statistics of the entire ensemble of passages, as we did for the maximum and mean wake velocity (Fig. 6), the 19 passages of the skater are clustered into the representative skating phases: The four different line types represent the four different phases in which the skater passes through the measurement plane. These four phases are also marked in Fig. 2. For readability, only the error bars on phase 2R are included being representative for phases 5L and 1R as well. From phase 4L, only one passage has been collected.

From the lateral wake's CG location (Fig. 7-left), a first observation is on the offset between the average wake's CG at X = 0 with respect to the skaters lower back. These offsets per skating phase are [3 –41 -53-75] mm for phases [4L 5L 1R 2R], respectively. In all skating phases except phase 4L, the wake's CG is located a few centimeters to the left of the lower back (it is located at higher negative Y′ values). In phase 4L (solid black line) this offset is about zero. In Fig. 7-left, it is also observed that the lateral location of the center of gravity of the wake changes with increasing distance to the rider (increasing X). In phase 4L (solid black line) it increases within 1 s, or 11 m assuming a quasi-steady wake, from zero to a maximum of about 6 cm. In the other phases, it decreases from around −5 cm to −12cm. Despite the difference in the evolution of the wake's CG location between phase 4L and the other three, also these displacements are all relatively small in comparison to the maximum lateral displacement of the skater itself, which is in the order of 2 m during one skating stroke (van der Kruk, 2018). In the next section, the change in drag reduction with increasing longitudinal and lateral offset between skaters is discussed and it will become more evident how relevant these small lateral offsets of the wake are.

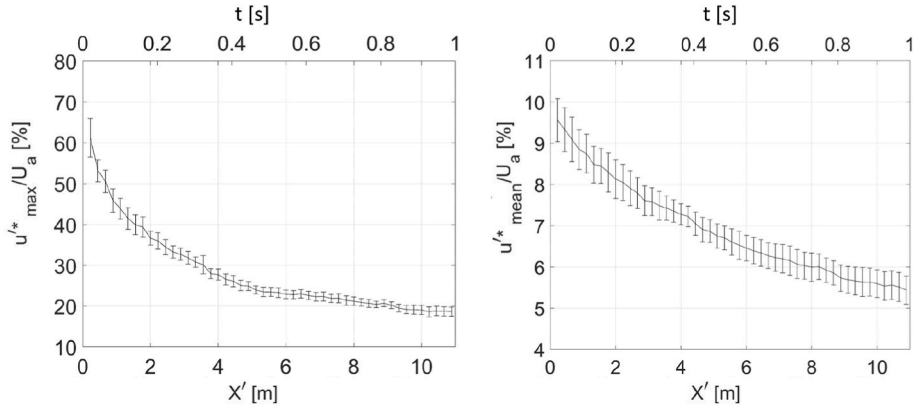

Fig. 6. Variation of the maximum (left) and average streamwise wake velocity downstream of the skater (right) at increasing distance to the rider.

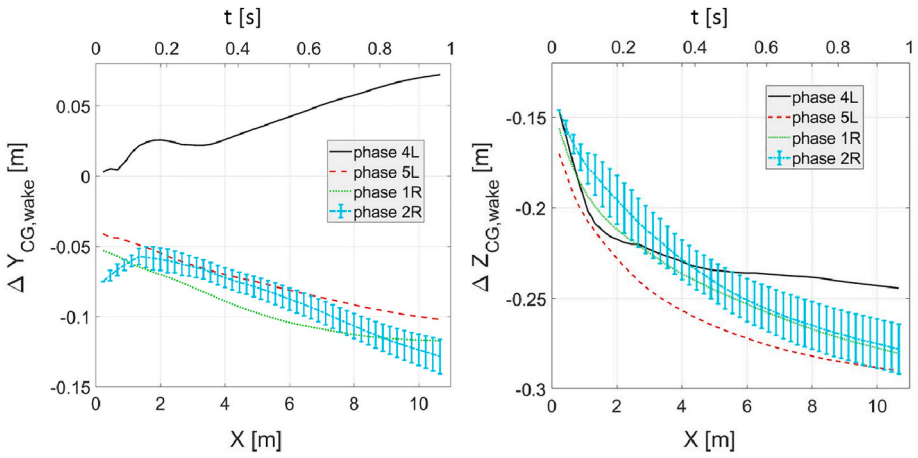

Fig. 7. Variation of the lateral location (left) and vertical location (right) of the skater's wake center of gravity with increasing distance to the rider. The wake location is relative to the location of the rider's lower back.

From the vertical location of the wake's CG (Fig. 7-right), it is observed that the initial offset between the CG and the lower back is about 15 cm: The wake's CG is about 15 cm below the lower back at X = 0. With increasing X, the vertical location of the wake's CG moves towards the floor for all skater phases. It decays about 12 cm within 1 s, so between X = 0 and X = 11 m. This downward motion was expected based on the qualitative description of the wake presented in Fig. 5. Apart from this decay, no significant correlation is observed between the magnitude of the decay and the phase in which the skater passed the measurement plane. The change in vertical location of the wake may not be exploited by a trailing skater for drag minimization. The fact that the wake moves closer to the ice floor does suggest, however, that shorter skaters benefit more from drafting than taller skaters do. This hypothesis is not further investigated in the present work.

For the estimation of the aerodynamic drag reduction by drafting through Equation (5), the total pressure in the wake is required. The dynamic pressure is directly obtained from the measured velocity. Instead, the static pressure is indirectly obtained from the velocity solving the Poisson equation for pressure (van Oudheusden, 2013) prescribing Neumann boundary conditions. Fig. 8 depicts the total pressure coefficient, $C_{p,tot}$ downstream of the skater in phases 4L (left) and 2R (right). The distribution of $C_{p,tot}$ is similar to that of the streamwise velocity (Fig. 5 top): A low pressure region is observed downstream of the hips and lower back, while away from the wake center, the total pressure equals that of the freestream. In parts of the domain, the total pressure slightly exceeds the freestream condition ($C_{p,tot} > 1$), which is physically not possible. This small error in the total pressure (<5%) stems from the evaluation of the static pressure, which is known to be sensitive to the prescribed boundary conditions.

4.3. Aerodynamic drag reduction

An estimation of the drag reduction by drafting in long track speed skating is provided, firstly, based on the Ring of Fire wake measurements on a single athlete and, secondly, through balance measurement on scaled, static skater models in a wind tunnel. Regarding the Ring of Fire measurements on the ice rink, it was observed that the streamwise velocity distribution downstream of a rider remains at a relatively fixed lateral position in the frame of reference fixed to the ice rink (Figs. 5 and 7). Hence, it is expected that the drag reduction through drafting peaks when a trailing rider follows the same trajectory on the ice as the leading one. To assess this, the drag reduction that would be experienced by a potential second rider is estimated using Equation (5). Note that this equation is evaluated in the frame of reference of the skater and so, to interchange time and distance between this frame of reference and the static one, it is assumed the wake is quasi-steady. The frontal area of the trailing rider is modelled by an ellipse with axes a (height) and b (width), as depicted in Fig. 8 right. This ellipse represents an average of the projected frontal area of the skater over an entire skating stroke. The ellipse height is equal to the height of the rider in the skating posture, while b is chosen such that the area of the ellipse matches the frontal area of the skater: [$a = 104$ cm; $b = 32$ cm] and [$a = 85$ cm; $b = 35$ cm] for the high trunk and low trunk configurations, respectively. Note that the ellipse of Fig. 8 is located in an arbitrary lateral position with respect

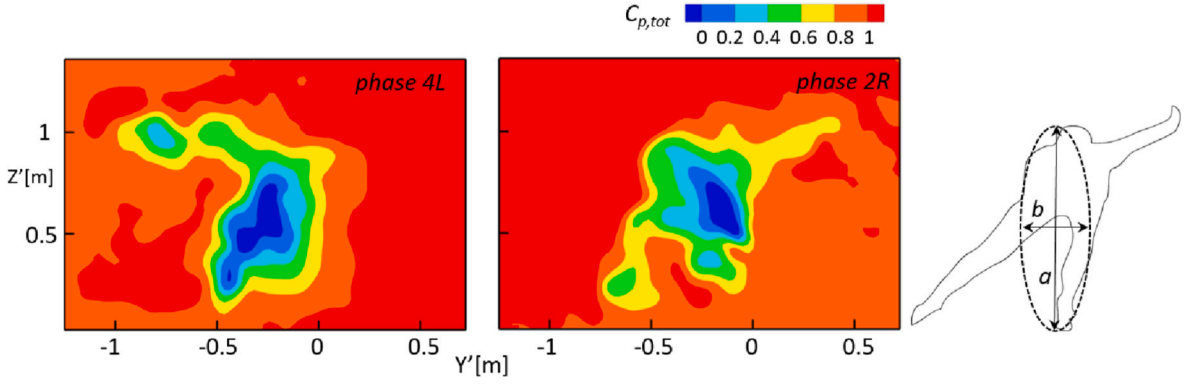

Fig. 8. Total pressure downstream of the skater at X = 0.5 m in phase 4L (left) and phase 2R (right). The frontal area, used for the estimation of a potential trailing skater, is marked by the black dashed ellipse.

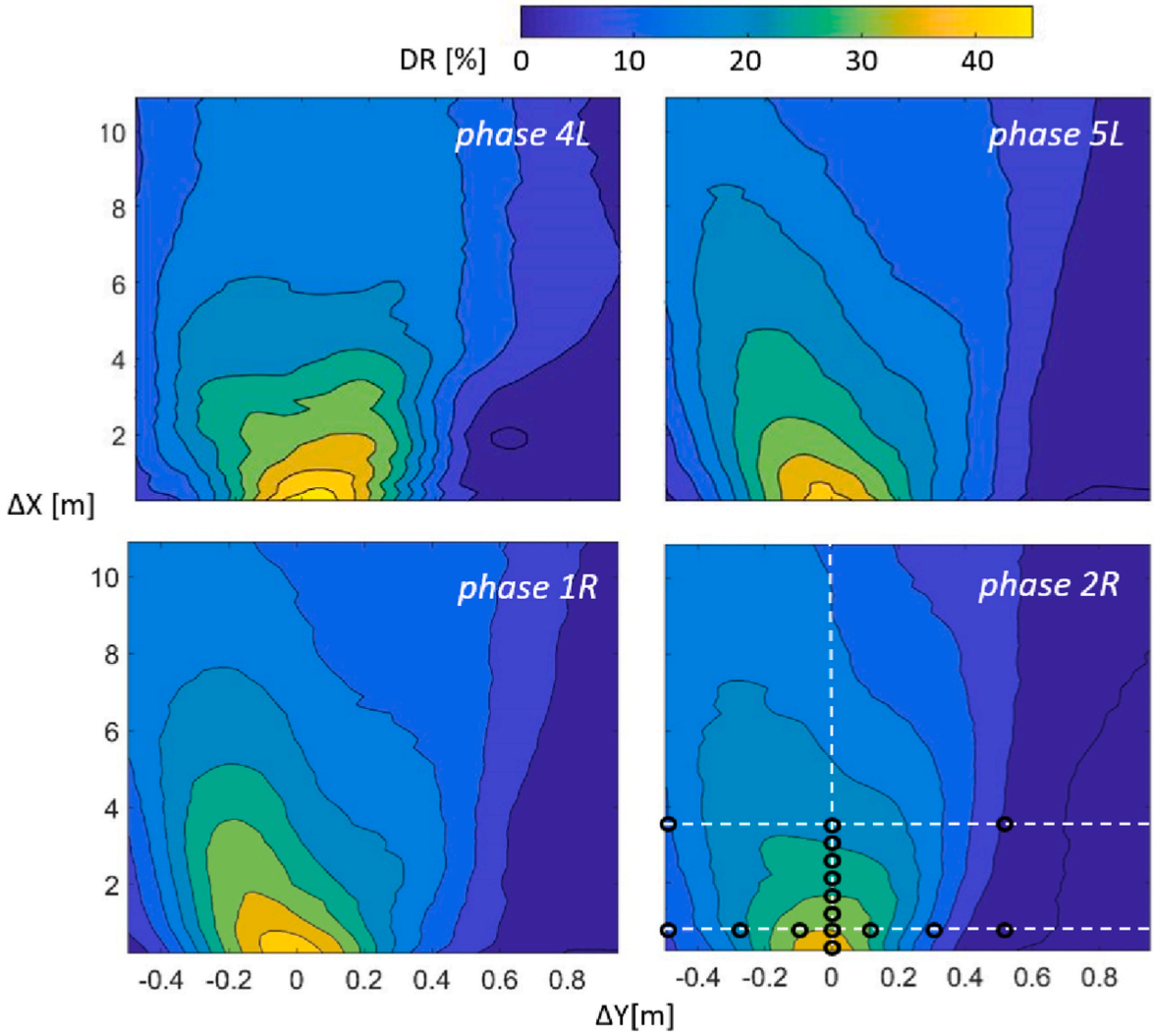

Fig. 9. Drag reduction estimates for four skating phases at different longitudinal and lateral offsets. The locations of the corresponding drag reductions from the wind tunnel tests are marked by black circles at the bottom-right.

to the skater's wake. For the evaluation of the aerodynamic drag reduction, the longitudinal position of this ellipse as well as the lateral one are varied in order to obtain a map of the drag reduction in a wide range of longitudinal and lateral distances (Fig. 9). An axis indicating time is omitted here. As expected, the drag reduction peaks at $\Delta X = 0$ and $\Delta Y = 0$, with a value around 40%. This peak reduction of a trailing skater downstream of a leading one in phase 4L (~45%, top-left) exceeds that of the other skating phases (~35%). The peak drag reduction decays quickly at increasing or decreasing ΔY. At close longitudinal distance to a trailing skater ($\Delta X = 0$), the drag reduction of a trailing rider is already negligible at a lateral offset between riders of 50 cm ($\Delta Y = \pm 50$ cm). For an optimal drag reduction of a trailing skater, it is therefore crucial to remain well aligned with the leading one.

Longer after the passage of a leading skater or at larger longitudinal offset (assuming quasi-steady wake), the effect of lateral offset changes. The peak drag reduction decays with increasing ΔX and, at the same time, it moves laterally. In the case that a skater passed in phase 4L, this lateral displacement is towards positive ΔY. Instead, for the other phases, the peak moves in negative ΔY direction. The direction of the lateral displacement corresponds to the direction of the lateral displacement of the wake center of gravity (see Fig. 7-right). Its magnitude, instead, exceeds that of the displacement of the wake center of gravity by about a factor 3: the displacement of the peak drag reduction at $X = 10$ m in phase 2R is about $\Delta Y = -20$ cm (Fig. 9 bottom-right), while the lateral displacement of the wake CG is $\Delta Y_{CG,wake} = -6$ cm (Fig. 7-right). At this large distance downstream of a skater, the wake is relatively wide and the drag reduction does not decay as strongly along the lateral direction as in the near wake. Nevertheless, with a lateral offset of 20 cm from the centre of the leading skater, the drag reduction decays by about 5%. Hence, for an optimal drag reduction of a trailing skater, the best strategy is to account for the lateral displacement of the peak drag reduction among the skating phases. In the phases where the skater is close to the centerline of its skating trajectory (phases 3 and 4; see Fig. 2) this offset is about zero, while in the phases where the skater is at larger distance to the centreline (phases 1, 2 and 5) this offset is in the same direction as the lateral distance to the centreline. This suggests that a trailing skater should follow a trajectory that is slightly wider than the leading one. At close longitudinal distance between the skaters, the trajectory should only be a few centimeters wider. Instead, at 10 m downstream of a leading skater, the trajectory should be a total of 40 cm wider (20 cm to the left and 20 cm to the right).

4.4. Comparison between on-site and wind tunnel measurements

In this paragraph, the drag reduction estimations from the in-field single-rider measurements are compared to those obtained in the wind tunnel on a tandem of scaled skater models. Fig. 10 depicts the estimated drag reduction from the wake measurements on the ice of Thialf,

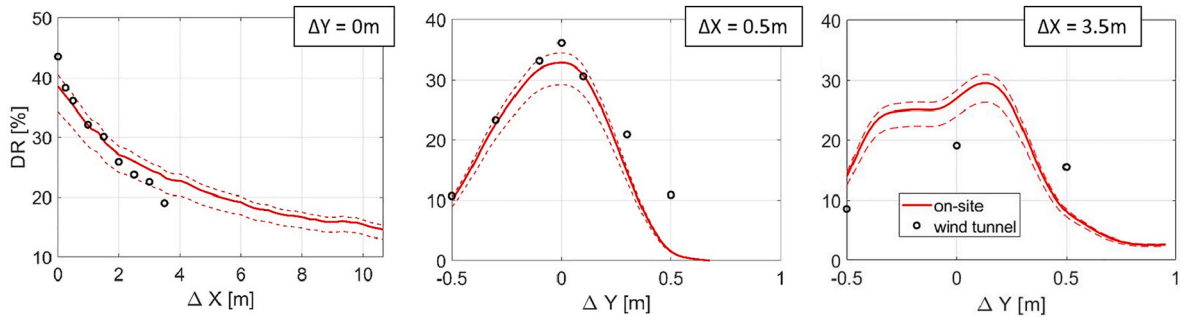

Fig. 10. Drag reduction estimates from the Ring of Fire data vs. wind tunnel balance measurements.

averaged over all skating phases (red lines) including the upper and lower uncertainty level (dashed), and the balance measurements in the wind tunnel (black circles). In the latter case, the drag reduction is computed using Equation (2). The corresponding longitudinal and lateral offsets between the two skater models in the wind tunnel are indicated by the black circles in Fig. 9 bottom-right. It is observed that the drag reduction at increasing ΔX ($\Delta Y = 0$; Fig. 10-left) of both methods overlaps within the uncertainty band, except at $\Delta X = 0$ m and $\Delta X = 3.5$m. At $\Delta X = 0$ m, so with a small distance between the skaters, the drag reduction from the wind tunnel exceeds that of the value obtained in the field. In the latter case, it is the other way around.

When comparing the two measurements at $\Delta X = 0.5$m (middle figure), it is observed that both the peak reduction at $\Delta Y = 0$ and the decay of the reduction at increasing $|\Delta Y|$ are well comparable. At $\Delta Y = 0$m, the drag reduction is 33%, while the value measured by force balance is 36%. At $\Delta Y = -0.3$m, the two methods provide an equal drag reduction of 23%, while, at $\Delta Y = +0.3$m the two are different (21% in the field vs 16% in wind tunnel). At larger longitudinal distance ($\Delta X = 3.5$m, right figure) the methods are further apart (30–50%) and, in particular, asymmetries with respect to $\Delta Y = 0$m are present in both results. In general, it is expected that the drag reduction estimation through Equation (5) is more reliable at larger longitudinal distance because of the widening of the wake, resulting in a more uniform flow field and the larger difference between the speed of the skater and the wake streamwise velocity (Jones, 1936; Brown et al., 2020). Instead, in the present case, the match between the two methods is rather independent of the longitudinal distance between the models.

5. Discussion

To provide a better understanding of the effect of drafting in speed skating, the wake of an isolated skater is characterized and used to estimate the drag reduction of a hypothetical trailing skater. As observed before by Spoelstra et al. (2022), clear differences exist among the different skating phases in the near-wake streamwise velocity and vorticity distribution. These differences in distributions are directly related to the changes in body position along the skating motion. In contrast to these distributions, the average and maximum streamwise velocities along the wake are very similar. This suggests that the drag reduction of a trailing skater is of the same order in all skating phases, which is confirmed by the aerodynamic drag estimations, which are between 35% and 45% at close longitudinal distance between two riders, and between 16% and 18% at 10 m distance. To achieve these peak drag reductions for a trailing skater, the present results suggests that the trailing skater's trajectory should be slightly wider than that of the leading one (about 40 cm at a longitudinal distance of 10 m). It should be noted that the latter relies on the assumption of a quasi-steady wake and that further research is required to understand the implications of it. Furthermore, when changing the skating trajectory may prove technically difficult, the drag reduction by drafting only decays by a few percent when the trailing skater's trajectory would be the same as that of the leading one. A further investigation into the lateral displacement of a skater's wake would be valuable, in particular for short track skating. In this discipline, the curves are quite steep, and so the effect of the lateral wake displacement may be more significant for a trailing skater. The present experiment also lacks statistical convergence; only a couple of skater passages were availed per skating phase for the wake analysis and drag reduction estimation. In fact one of the five phases is missing at all in the present dataset (phase 3) and for phase 4 only a single passage was collected. A new experimental campaign designed specifically for a skater to pass through the Ring of Fire in all the different phases, towards the left and the right, is therefore recommended.

The present in-field measurements provide new insights on the effect of drafting in speed skating, in particular, because they have been executed on an ice rink with an actual skater. One difference between the present experimental conditions and those experienced in a race is the injection of flow tracers. This injection slightly disturbs the air in the measurement region. Although the effect of the injection on the flow around the skater is negligible in the part of the measurement domain where the skater passed (Spoelstra et al., 2022), it may affect the air conditions when installing the seeding system differently or when using another seeding system in the future.

The method of estimating the aerodynamic drag from the wake of an isolated skater provides results closely matching those obtained in a wind tunnel experiment in a 1:5 scale static skater mannequin. While this method is expected to predict the drag reduction more accurately in the far wake, the present results, instead, match the wind tunnel data closer in the near wake. At a close distance from the skater, it can be argued that the dynamic effects of the motion of the skater (changing velocity and orientation of the legs and the arms) are small, and therefore a good agreement with the static balance measurement results is retrieved. Instead, at larger distances, the wake development is affected to a larger extent by the dynamic motion of the skater. For this reason, larger discrepancies between balance measurements and ice-rink measurements occur. Independent of the position in the wake, it should be noted that there are quite some differences in experimental conditions between the measurements on the ice rink and in the wind tunnel, among others the geometry and posture of the skater, the governing Reynolds number and the surface of the skater (the athlete was wearing a suit). All these factors may affect the present comparison. A dedicated study on the reliability of the drag estimation method is recommended, which, among others, compares the methods' estimates to balance data obtained from the same models in a wind tunnel.

Nevertheless, the order of magnitude of the present drag reduction predictions are likely close to those that are experienced by an actual trailing skater. Hence, the results are relevant in a variety of different skating situations. For example, in all the team disciplines in which a rider skates closely behind a leading rider (e.g. team sprint and team pursuit). In these situations, he or she should remain aligned with the skater in front, as it is observed that the drag reduction decays quickly with a lateral offset between riders. The present results are also valuable when two riders in individual disciplines change of lanes. During this

moment, the skater that crosses lanes downstream can benefit from the leading rider best when skating along the same trajectory, also when there is a significant gap (>10 m) between the riders. Finally, the present quantitative results of drafting may help the International Skating Union (ISU) to regulate more fairly these sprint races. In such races, skaters cross lanes only one time and, so, only one of the riders can benefit from drafting. With the present drag reduction values, they may, for example, decide whether to organise a single 500 m event or have two 500 m races, where a rider once starts in the outer and once in the inner lane.

6. Conclusions

Experiments on the 400m ice rink of Thialf are conducted to investigate the effect of drafting in speed skating. The wake of a single rider is characterized using the Ring of Fire system. This system adopts large-scale stereoscopic PIV to measure the three velocity components in a plane orthogonal to the direction of the skating lane. During the experiments, a skater repeatedly transits through the Ring of Fire to acquire statistical wake data up to 11 m after passing the measurement plane. From individual transits of the skater, passing in different skating phases, it is evident that the distribution of streamwise velocity and vorticity in the near wake is governed by the skater's posture. In the far wake, differences between the skating phases (skater postures) diminish. The location of the wake is quantified using the wake's center of gravity. It is observed that in all skating phases the wake moves about 15 cm to the ice floor over a longitudinal distance of 10 m. Laterally, it displaces about 6 cm when the skater passes in a position (phases 1, 2 and 5) that is relatively far from the centreline of its harmonic trajectory. Instead, in phase 4, when the rider is crossing the centreline, this lateral displacement is negligible.

The estimated drag reduction peaks (35–45%) when the longitudinal and lateral distance between two riders is minimum. This estimated drag reduction strongly decays with increasing lateral offset. These findings are confirmed by wind tunnel experiments conducted on 1:5 scale skater models. In comparison to the lateral decrease, the drag reduction decays less steep with increasing longitudinal distance between the riders. At an offset of 10 m the peak value is around 17%. In the phases where the wake's CG moved laterally at increasing longitudinal offset, also the location of this peak drag reduction value has shifted by about 20 cm. Hence, to achieve an optimal drag reduction for a trailing skater, his or her trajectory should be slightly wider than that of the leading skater. If, however, the same trajectory is followed, the drag reduction does not suffer much and decreases by only a few percent.

Author statement

Wouter Terra: Conceptualization; Data curation; Formal analysis; Software; Validation; Visualization; Roles/Writing – original draft; Writing – review & editing; Resources; **Andrea Sciacchitano**: Funding acquisition; Conceptualization; Methodology; Supervision; Writing – review & editing, **Alexander Spoelstra**: Investigation; Methodology; Data curation; Software;

Declaration of competing interest

The authors declare that they have no known competing financial interests or personal relationships that could have appeared to influence the work reported in this paper.

Data availability

The data underlying the present manuscript will be uploaded to the 4TU repository.

Acknowledgments

This research is supported by the Dutch National Olympic Committe (NOC*NSF), the Dutch Skating Federation (KNSB) and Innovatielab Thialf. The support of all participating staff and athletes is kindly acknowledged.

Appendix

This appendix contains details of all individual passages, in the order as executed on the ice rink, of the skater through the Ring of Fire. Each passage is categorized into a particular skating phase and into a skating configuration with a low or a high trunk. Furthermore, for each passage the vertical and lateral position of the lower back and the head are listed and as well the location of the computed wake's CG.

Passage	Phase	Trunk Config	Location lower back		Location head		Location wake's CG at X = 0	
		H(igh)/L(ow)	Z′ [mm]	Y′ [mm]	Z′ [mm]	Y′ [mm]	Z′ [mm]	Y′ [mm]
1	1R	H	759	−915	984	−854	630	−948
2	2R	L	719	−721	852	−740	588	−792
3	2R	H	796	−408	978	−436	668	−465
4	1R	L	698	−835	818	−829	571	−888
5	2R	H	769	−592	1027	−638	663	−720
6	2R	L	722	−835	855	−857	546	−921
7	5L	H	766	−1173	1015	−1075	593	−1186
8	1R	L	725	−1011	855	−974	503	−1066
9	1R	H	738	−977	1033	−927	615	−1018
10	5L	L	716	−1087	827	−1000	551	−1160
11	2R	H	787	−672	975	−694	652	−753
12	1R	L	735	−1054	830	−1044	580	−1136
13	1R	H	756	−1057	978	−946	569	−1111
14	2R	L	738	−762	815	−804	572	−840
15	5L	H	771	−927	1033	−841	591	−989
16	5L	L	722	−934	839	−897	548	−978
17	5L	H	774	−1060	1048	−998	614	−1091
18	5L	L	738	−1177	830	−1139	566	−1198
19	4L	H	787	−833	1051	−734	640	−829

References

Barry, N., Sheridan, J., Burton, D., Brown, N.A.T., 2014. The effect of spatial position on the aerodynamic interactions between cyclists. Procedia Eng. 72, 774–779.

Barry, N., Burton, D., Sheridan, J., Thompson, M., Brown, N.A.T., 2015. Aerodynamic drag interactions between cyclists in a team pursuit. Sports Eng. 18, 93–103. https://doi.org/10.1007/s12283-015-0172-8.

Barry, N., Burton, D., Sheridan, J., Thompson, M., Brown, N.A.T., 2016. Flow field interactions between two tandem cyclists. Exp. Fluid 57, 181. https://doi.org/10.1007/s00348-016-2273-y.

Belloli, M., Giappino, S., Robustelli, F., Somaschini, C., 2016. Drafting effect in cycling: investigation by wind tunnel tests. Procedia Eng. 147, 38–43.

Blocken, B., Defraeye, T., Koninckx, E., Carmeliet, J., Hespel, P., 2013. CFD simulations of the aerodynamic drag of two drafting cyclists. Comput. Fluids 71, 435–445.

Blocken, B., et al., 2018. Aerodynamic drag in cycling pelotons: new insights by CFD simulation and wind tunnel testing. J. Wind Eng. Ind. Aerod. 179, 319–337.

Broker, J.P., Kyle, C.R., Burke, E.R., 1999. Racing cyclist power requirements in the 4000-m individual and team pursuits. Med. Sci. Sports Exerc. 31 (11), 1677–1685. https://doi.org/10.1097/00005768-199911000-00026.

Brown, C., Crouch, T., Burton, D., Thompson, M.C., 2020. Understanding the aerodynamic benefits of drafting in the wake of cyclists. In: Proceedings, vol. 49, p. 32.

Crouch, T.N., Burton, D., Brown, N.A.T., Thomson, M.C., Sheridan, J., 2014. Flow topology in the wake of a cyclist and its effect on aerodynamic drag. J. Fluid Mech. 748, 5–35.

Howland, M.F., Bossuyt, J., Martínez-Tossas, L.A., Meyers, J., Meneveau, C., 2016. Wake structure in actuator disk models of wind turbines in yaw under uniform inflow conditions. J. Renew. Sustain. Energy 8, 043301.

Huang, M., Sciacchitano, A., Ferreira, C., 2022. On the wake deflection of vertical axis wind turbines by fixed-pitched blades. J. Wind Energy. Under review in.

Jones, B, 1936. Measurement of Profile Drag by the Pitot-Traverse Method. ARC R&M 1688.

Oggiano, L., Sætran, L., 2010. Experimental analysis on parameters affecting drag force on speed skaters sport. Technol. 3, 223–234.

Rundell, KW, 1996. Effects of drafting during short-track speed skating. Med. Sci. Sport. Exerc. 28 (6), 765–771.

Sciacchitano, A., Scarano, F., Wieneke, B., 2012. Multi-frame pyramid correlation for time resolved PIV. Exp. Fluid 53, 1087.

Spoelstra, A., de Martino Norante, L., Terra, W., Sciacchitano, A., Scarano, F., 2019. On-site cycling drag analysis with the Ring of Fire. Exp. Fluid 60 (6), 90. https://doi.org/10.1007/s00348-019-2737-y.

Spoelstra, A., Hirsch, M., Sciacchitano, A., Scarano, F., 2020. Uncertainty assessment of the Ring of Fire concept for on-site aerodynamic drag evaluation. Meas. Sci. Technol. 32, 044004.

Spoelstra, A., Sciacchitano, Andrea, Scarano, Fulvio, Mahalingesh, Nikhil, 2021. On-site drag analysis of drafting cyclists. J. Wind Eng. Ind. Aerod. 219, 104797.

Spoelstra, A., Terra, W., Sciacchitano, A., 2022. On-site aerodynamics investigation of speed skating. J. Wind Eng. Ind. Aerod. *Under review in*.

Terra, W., Spoelstra, A., Sciacchitano, A., 2022. Data Underlying the Work: Aerodynamics Analysis of Speed Skating Helmets: Investigation by CFD Simulations. 4TU Repository.

Van den Brandt, F.A.P., Stoter, I.K., Otter, R.T.A., Elferink-Gemser, M.T., 2021. Why train together when racing is performed alone? Drafting in long-track speed skating. Int. J. Sports Physiol. Perform. 16 (12), 1874–1879.

Van der Kruk, E., 2018. Parameter Analysis for Speed Skating Performance. PhD Thesis. repository TU Delft.

Van Ingen Schenau, G.J., 1982. The influence of air friction in speed skating. J. Biomech. 15 (6), 449 458.

Van Oudheusden, B.W., 2013. PIV-based pressure measurement. Meas. Sci. Technol. 24 (3), 032001.